

X 頻帶雙飄移高低高砷銜渡二極體之準靜態設計規範

Quasi-Static Design Considerations of X-Band Double Drift Lo-Hi-Lo Silicon IMPATT Diodes

張懋中, 陳茂傑 Mau-Chung Chang & Mao-Chieh Chen

The Institute of Electronics, N.C.T.U.

(Received October 19, 1976)

ABSTRACT — A modified quasi-static model is developed to optimize the power efficiency of double-drift X-Band Lo-Hi-Lo IMPATT diodes. We take the ionization rates and scattering-limited velocities for electrons and holes to be not equal at an operation temperature of 150°C, and let the carriers' ionization coefficient be in the form  $\alpha = A \cdot \exp(-B/E)$ , where E is the electric field. We maintain the carriers' velocities at saturation and solve for a steady state solution. All these assumptions not only save computer time, but also give us essential physical features. Current tuning effect is concluded as the most important factor in designing the device structure. Large signal values of negative conductance, susceptance, r.f. power generation efficiency are calculated as a function of the oscillation voltage amplitude for a specified bias current density. All of these informations would provide a useful guidance for both device and circuit designers.

## I. Introduction

Early works in treating the large-signal analysis of IMPATT diodes are generally either too costly or too restrictive to be useful in the practical device design. By using a quasi-static technique, Kuvás and Lee [1] generalized the applicability of the Read-type model by removing several of the simplified assumptions made by Blue [2] and Haddad & Evans [3] that had shown an ordinary differential equation of the same form characterizing the device performance. Their generalizations include the effects of unequal ionization rates and unequal scattering-limited velocities for electrons and holes respectively and also include the carrier-induced displacement current in the avalanche zone. By combining the numerical technique of Blue's with the quasi-static formulation developed by Kuvás and Lee, Decker [4] has accomplished this synthesis to arbitrary field profiles. This paper presented here basically follows the work developed by Decker, but makes further modification in phase derivations and is applied to the designing of the double drift X-Band Lo-Hi-Lo silicon IMPATT diodes. Meanwhile, under some degenerate conditions ( $v_n = v_p = v, \alpha = \beta = \alpha$ ), we compare the quasi-static results with that of Blue's and those derived from the small signal model.

## II. Mathematical Analysis

The doping profile of a double drift Lo-Hi-Lo silicon diode is depicted in Fig. 1 (a), where  $X$  and  $\delta$  are the depth and width of the buried-layer respectively. Fig. 1 (b) shows the electric field distribution for punch-through

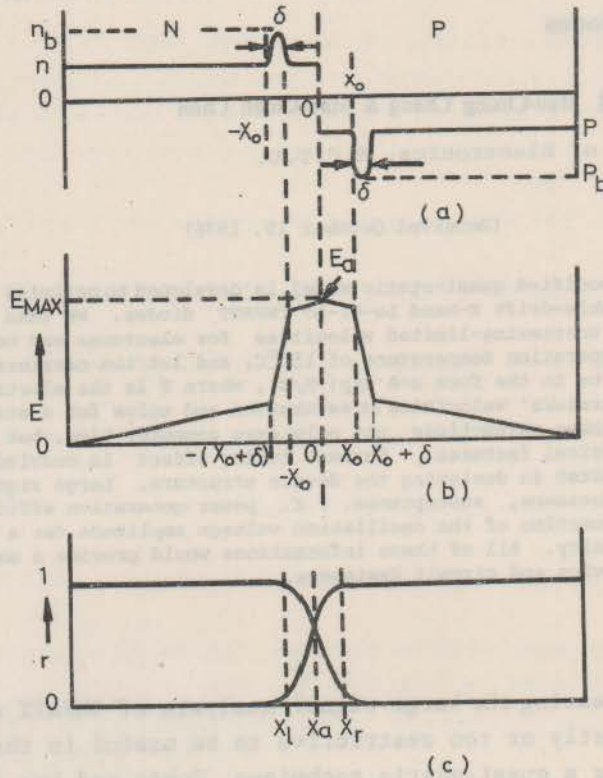


Fig. 1. Double-Drift Lo-Hi-Lo IMPATT diode. The avalanche zone is shifted to the n-side.

double-drift Lo-Hi-Lo IMPATT diode at low injection condition and is given by

$$E_1(x) = E_c - \frac{qn_x}{\epsilon_s} \quad 0 \leq x \leq x_0 \quad (1)$$

$$E_2(x) = E_c + \frac{qp_x}{\epsilon_s} \quad -x_0 \leq x < 0 \quad (2)$$

$$E_3(x) = E_1(x_0) - \frac{qn_b(x-x_0)}{\epsilon_s} \quad x_0 \leq x \leq x_0 + \delta \quad (3)$$

$$E_4(x) = E_1(-x_0) + \frac{qp_b(x+x_0)}{\epsilon_s} \quad -(x_0 + \delta) \leq x < -x_0 \quad (4)$$

$$E_5(x) = \frac{qn(W-x)}{\epsilon_s} \quad x_0 + \delta \leq x \leq W \quad (5)$$

$$E_0(x) = \frac{qp(W+x)}{\epsilon_s} \quad -W \leq x \leq -(x_0 + \delta) \quad (6)$$

where  $n$  &  $p$  are the concentrations of the background doping, and  $n_b$  &  $p_b$  are the concentration of the buried-layer for each side. Assume a symmetric double-drift structure, we have  $n=p$  and  $n_b=p_b$ . From equations (1), (3) and (5), the width of the buried layer is found to be

$$\delta = \frac{E_c - \frac{qnW}{\epsilon_s}}{\frac{q}{\epsilon_s}(n_b - n)} \quad (7)$$

If  $n_b$  is much greater than  $n$ ,  $\delta$  is inversely proportional to  $n_b$  for a fixed depletion width  $W$ . In the avalanche zone (Fig. 1 (b)), holes move in the positive  $x$ -direction, and if the scattering-limited velocity is assumed well saturated under avalanche condition, the time dependent continuity equations for both electrons and holes would take the following forms:

$$\frac{\partial i_n}{\partial t} - v_n \frac{\partial i_n}{\partial x} = (\alpha i_n + \beta i_p) v_n \quad (8)$$

$$\frac{\partial i_p}{\partial t} + v_p \frac{\partial i_p}{\partial x} = (\alpha i_n + \beta i_p) v_p \quad (9)$$

where  $i_n$  and  $i_p$  represent the electron and hole current density respectively;  $\alpha$  &  $\beta$ , the ionization rates of electrons and holes respectively, and  $v_n$  &  $v_p$ , the magnitude of the scattering-limited velocity of electrons and holes respectively. The saturated velocities of electrons and holes had been measured by Duh and Moll [5] at room temperature and 200°C. The extrapolation of their data to the 150°C region gives

$$V_n = 8.9 \times 10^6 \text{ cm/sec, and}$$

$$V_p = 1.06 \times 10^7 \text{ cm/sec}$$

in the high field approximation. If Equations (8) and (9) are combined and a quasi-static approximation is made, Kuvás and Lee [1] had derived the following salient equations

$$\left\{ \frac{\partial}{\partial t} + (M\tau_i)^{-1} - \lambda [\partial E(t) / \partial t] \right\} i = \left\{ \tau_i^{-1} - \lambda [\partial E(t) / \partial t] \right\} i_s \quad (10)$$

$$\tau_i = k\tau \quad (11)$$

$$M i_s = M_n i_{sn} + M_p i_{sp} \quad (12)$$

$$(i_s/\tau) = (i_{sn}/\tau_n) + (i_{sp}/\tau_p) \quad (13)$$

where  $\tau$  is the intrinsic response time,  $i_s$  the total reverse-saturation current of the diode.

Consider a double-drift IMPATT diode shown in Fig. 1, the multiplication factor for electron should be

$$M_n^{-1} = 1 - \int_{-W}^W \alpha \exp(-\int_x^W (\alpha - \beta) dx') dx \quad (14)$$

and the corresponding response time is

$$\tau_n = \int_{-W}^W \exp(-\int_x^W (\alpha - \beta) dx') (dx / (v_n + v_p)) \quad (15)$$

These quantities are related to the corresponding values of hole-initiated excitation by

$$M_n/M_p = \tau_p/\tau_n = \exp(\int_{-W}^W (\alpha - \beta) dx) \quad (16)$$

Here we note  $M_n \tau_n = M_p \tau_p$  as a time constant for the structure, and is independent of whether it is electron or hole excitation, i.e.

$$M_n \tau_n = M_p \tau_p = M\tau \quad (17)$$

Since the parameter  $\lambda$  appeared in (10) is very small and negligible, Decker [4] proved that the parameter  $K$  could be deduced to a simple form

$$K = \tau_p^{-1} (v_p^{-1} + v_n^{-1}) \int_{-W}^W r_n(x) r_p(x) \exp(\int_W^x (\alpha - \beta) dx') dx \quad (18)$$

where

$$r_p(x) = i_p(x)/i = [\exp(\int_{-W}^x (\beta - \alpha) dx')] \cdot \int_{-W}^x \alpha(x') \exp[-\int_W^{x'} (\beta - \alpha) dx''] dx' \quad (19)$$

and

$$r_n(x) = 1 - r_p(x) = i_n(x)/i \quad (20)$$

From Equation (17), the corrected multiplied response time could be derived in terms of Equation (18)

$$\begin{aligned} (M\tau_i)^{-1} &= (M_n K \tau_n)^{-1} = (M_p K \tau_p)^{-1} \\ &= \frac{1 - \int_{-W}^W \alpha (\exp \int_W^{x'} (\alpha - \beta) dx'') dx'}{(v_n^{-1} + v_p^{-1}) \int_{-W}^W r_n(x) r_p(x) (\exp \int_W^x (\alpha - \beta) dx') dx} \end{aligned} \quad (21)$$

In this equation,  $\alpha$  and  $\beta$  are functions of the dynamic field  $E(x,t)$ , and can be approximated in the form [6]:

$$\alpha = A \cdot \exp(-B/E) \quad \text{and} \quad \beta = C \cdot \exp(-D/E)$$

whereas  $r_n(x)$  and  $r_p(x)$  are kept at their dc values, and no further modification is made when oscillation voltage is applied. Because the total field is a combination of the dc field, the applied voltage and the space charge feedback due to the drifting carriers,  $E_t$  can be written as

$$E_t(x,t) = E_o(x) + E_a(t) + E_{sc}(x,t) \quad (22)$$

As we know  $E_o(x)$  is determined from dc break-down condition for the designed structure and at some specified bias current density. The applied electric field is obtained from the applied driving voltage divided by the total depletion width

$$E_a(t) = V_a(t) / 2W \quad (23)$$

The space-charge induced electric field is given from the Poisson equation and could be shown as

$$E'_{sc}(x,t) = -\frac{1}{\epsilon_s} \int_x^w \left[ \frac{i_p(x,t)}{v_p} - \frac{i_n(x,t)}{v_n} \right] dx' \quad (24)$$

Therefore, when we define the space charge voltage  $V_{sc}$  as

$$V_{sc}(t) = \int_{-W}^W E'_{sc}(x,t) dx \quad (25)$$

it is necessary to subtract  $V_{sc}(t)/2W$  from  $E'_{sc}(x,t)$  before adding it to obtain  $E_t$ , since the desired terminal voltage is just the applied voltage, thus

$$E_{sc}(x,t) = E'_{sc}(x,t) - V_{sc}(t)/2W \quad (26)$$

The individual particle current  $i_p$  and  $i_n$  are calculated based on the assumptions that

- (1) the current fraction derived from dc solution is approximately correct;
- (2) the phase shift for each particle current relative to the avalanche current is calculated with respect to the total particle current at the center of the avalanche zone.

Therefore, we have

$$i_p(x,t) = r_p(x) \cdot i \left( t - \frac{x-x_a}{v_p} \right) \quad (27)$$

$$i_n(x,t) = (1-r_p(x)) \cdot i \left( t + \frac{x-x_a}{v_n} \right) \quad (28)$$

where  $x_a$  is the position where the peak generation of carriers occurs.

The external current is calculated by spatially averaging the particle current in the depletion region and adding to it the displacement current where

$$i_e = i_c + i_d$$

$$= \frac{1}{2W} \left\{ \int_{-W}^W (i_p(x', t) + i_n(x', t)) dx' + \epsilon_s \frac{dV_a}{dt} \right\} \quad (29)$$

the first term is the external conduction current and the second term the displacement current. If the sinusoidal perturbation is applied, then

$$V_a(t) = V_{rf} \cdot \sin \omega t \quad (30)$$

Through Fourier analysis, we have the conductance  $G(\omega)$  and the susceptance  $B(\omega)$  as follows:

$$G(\omega) = \frac{2}{TV_{rf}} \int_0^T i_c(t) \cdot \sin \omega t \, dt \quad (31)$$

$$B(\omega) = \frac{2}{TV_{rf}} \int_0^T i_e(t) \cdot \cos \omega t \, dt \quad (32)$$

where  $T$  represents the period of oscillation, and in Formula (31), only the external conduction current  $i_c(t)$  appears in the integrand because the displacement current  $i_d$  does not contribute to the conductance  $G(\omega)$ . If the small value of  $\lambda$  is negligible, Eq. (10) can be simplified to read

$$[d/dt + (M\tau_i)^{-1}] i = i_s / \tau_i \quad (33)$$

From above,  $i(t)$  can be solved as

$$i(t) = \exp(-\int_0^t (M\tau_i)^{-1} dt) \cdot \{ i(0) + (i_s / \tau_i) \int_0^t \exp(\int_0^{t'} (M\tau_i)^{-1} dt'') \} \quad (34)$$

The inverse response time  $(M\tau_i)^{-1}$  appears as an exponential growth factor for the particle current and under the condition that the total reverse-saturation current is insignificantly small, the particle current is reduced to

$$i(t) = i(0) \cdot \exp(-D(t)) \quad (35)$$

with

$$D(t) = \int_0^t (M\tau_i)^{-1} dt \quad (36)$$

Using the numerical procedure similar to that of Blue's, we can solve this system more accurately and more generally. It is not necessary to assume equal drift velocities and ionization rates which are only suitable for certain kinds

of semiconductor material, and it is also not necessary to assume a uniform avalanche electric field which exists only in an idealized Read diode.

### III. Numerical Considerations

For the sake of clarity, some of the numerical details are omitted in the discussion. First, we adjust static field  $E_0(x)$  so that the breakdown condition

$$\int_{-W}^W \alpha(E_0) \exp \int_W^{x'} (\alpha(E_0) - \beta(E_0)) dx'' dx' = 1 \quad (37)$$

is fulfilled for a specified diode structure and the desired dc bias current. The depletion width  $W$  is determined by the operation frequency  $W(\mu) = 33/f(\text{GHz})$  for silicon at  $150^\circ\text{C}$  [7]. Since the ionization rate of electrons differs from that of holes in silicon at a given temperature, Grant [8] derived a set of equations to fit his experimental data obtained at  $150^\circ\text{C}$  as follows:

$$\alpha = 1.37 \times 10^6 \exp(-1.48 \times 10^6/E) \quad \text{for } E < 2.16 \times 10^5 \text{ V/cm} \quad (38)$$

$$\alpha = 7.52 \times 10^5 \exp(-1.35 \times 10^6/E) \quad \text{for } E > 2.16 \times 10^5 \text{ V/cm}$$

For electrons, and

$$\beta = 1.31 \times 10^6 \exp(-1.92 \times 10^6/E) \quad \text{for } E < 6.07 \times 10^5 \text{ V/cm} \quad (39)$$

$$\beta = 6.89 \times 10^5 \exp(-1.53 \times 10^6/E) \quad \text{for } 6.07 \times 10^5 \text{ V/cm} < E < 6.74 \times 10^5 \text{ V/cm}$$

$$\beta = 3.28 \times 10^5 \exp(-1.03 \times 10^6/E) \quad \text{for } E > 6.74 \times 10^5 \text{ V/cm}$$

for holes.

Since the avalanche oscillators such as IMPATT diodes are operated from constant current power supplies, the dc bias current  $J_{dc}$  is taken as a bias parameter. In order to satisfy a specified bias current, the dc bias voltage  $V_{dc}$  has to be corrected from the breakdown value  $V_B$  by the relation

$$V_{dc} = V_B + (\Delta E_{op})(2W) \quad (40)$$

where "+" sign is for over punch through and "-" sign for under punch through operations respectively, and  $|\Delta E_{op}|$  is the amount of deviation from the break-

down field.

A dc solution of the current fraction  $r_n(x)$  and  $r_p(x)$  are evaluated with Equation (19) and (20). The peak generation position  $X_a$  is the position where the magnitude of current gradient

$$\left| \frac{\partial i_n}{\partial x} \right| = \left| \frac{\partial i_p}{\partial x} \right| = (\alpha i_p + \beta i_n) \quad (41)$$

has the maximum value.  $r_n(x)$ ,  $r_p(x)$  and  $X_a$  derived above are assumed approximately correct in the dynamic electric field case without any further modifications. For an applied voltage  $V_a(t)$ , the situation may be viewed as an initial-value problem where the response of the diode is determined simply from Equation (36). By properly assuming an initial current  $i(0)$ , the time evolution of avalanche current  $i(t)$  and external induced current  $i_c(t)$  could be computed iteratively. Practically the periodic steady state response  $i_c(t)$  to an applied voltage  $V_a(t)$  not the transient response from some arbitrary initial state, is of great interest. Therefore, in this work, the time integration is carried out after a steady state has been reached; the transient behavior is not discussed. The total time required to achieve the steady state is typically 10 r.f. periods. Each period is divided into a number of time steps (typically 50). The condition that the current response must be periodic leads to the average value of  $(M\tau_i)^{-1}$  over one period equal to zero, namely

$$D(T) = \int_0^T (M\tau_i)^{-1} dt = 0 \quad (42)$$

Therefore, after each computation cycle is finished, the  $n$ 'th run initial current  $i^n(0)$  should be replaced by  $i^{n-1}(T)$ . The procedure continues until a steady solution has been achieved, then for an prescribed infinitesimal value  $\xi$

$$|i^n(T) - i^{n-1}(0)| < \xi \quad (43)$$

is satisfied, and the current response for a given driving condition is hereby obtained. Again, by using Fourier integrals Equations (31) and (32),  $G(\omega)$  and  $B(\omega)$  are calculated for the final run. The r.f. power density can be written as

$$P_{rf} = \frac{1}{2} \cdot V_{rf}^2 \cdot G \quad (44)$$

and power efficiency  $\eta$  is equal to

$$\eta = \frac{P_{rf}}{J_{dc} \cdot V_{dc}} \times 100\% \quad (45)$$

where  $J_{dc}$  and  $V_{dc}$  are the dc bias current and voltage respectively. If more rapid convergence is desired, the conventional  $n$ -dimensional Newton-Raphson iteration method can be used, which is already well known and will not be described here.



#### IV. Results and Discussions

##### 1. Optimization design criterions with double-drift Lo-Hi-Lo doping profiles

Among various Lo-Hi-Lo doping profiles, two group of representative diodes are submitted to the quasi-static calculations without losing any generality. Table 1 gives the doping profiles of the diodes.

Table 1. Doping profiles of the diodes

Run No.	Single-side depletion width $W(\mu)$	depth of buried layer $x_o(\mu)$	$n_b/n(p_b/p)$	$n(p)(10^{16}/\text{cm}^3)$
1-a	3.3	0.1	100	0.51
1-b	3.3	0.1	200	0.51
1-c	3.3	0.1	400	0.51
2-a	3.3	0.1	100	0.58
2-b	3.3	0.1	200	0.58
2-c	3.3	0.1	400	0.58

The selected background concentration is 75 or 85 percent of the doping concentration of a uniformly doped double-drift diodes, which was deduced from Equations (37), (38) and (39) as  $0.68 \times 10^{16}/\text{cm}^3$  [9]. Diodes with background concentrations higher than 85% of the above mentioned value are proved to be very hard to oscillate in our program; and diodes with background concentrations lower than 75% of which might not be able to maintain the drift velocity saturation in the drift zone outlet. The depth of buried layer  $X_o=0.1\mu$  is chosen for the sake of easy fabrication (easy for ion implantation) as well as for a concentrated generation zone which benefits a sharper spectrum of phase delay for the avalanche current. The single-sided drift length  $W$  was postulated by Su and Sze [7] with small signal theory to be favorably convenient to operate at 10GHz in the small current limit. However, when the bias current increased, optimum frequency also ascends to a higher value due to the increasing space charge effect. This is easily seen in Fig. 2.

At any fixed operation frequency an IMPATT diode will have an optimum bias current at a fixed r.f. voltage swing. An efficiency v.s. dc bias current for a 20% modulation (modulation index  $m=5$ ) at 12.5GHz is shown in Fig. 3. It is seen that  $750\text{A}/\text{cm}^2$  is the most favorable bias condition for the group -2 diodes, while those of the group -1 diodes are around  $600\text{A}/\text{cm}^2$ . It seems that the optimum bias condition is much sensitive to the background concentration  $n(p)$  than to the ratio  $n_b/n(p_b/p)$  which agrees with that of the small signal theory derived by Gilden and Hince [10] that the avalanche resonance frequency is given by

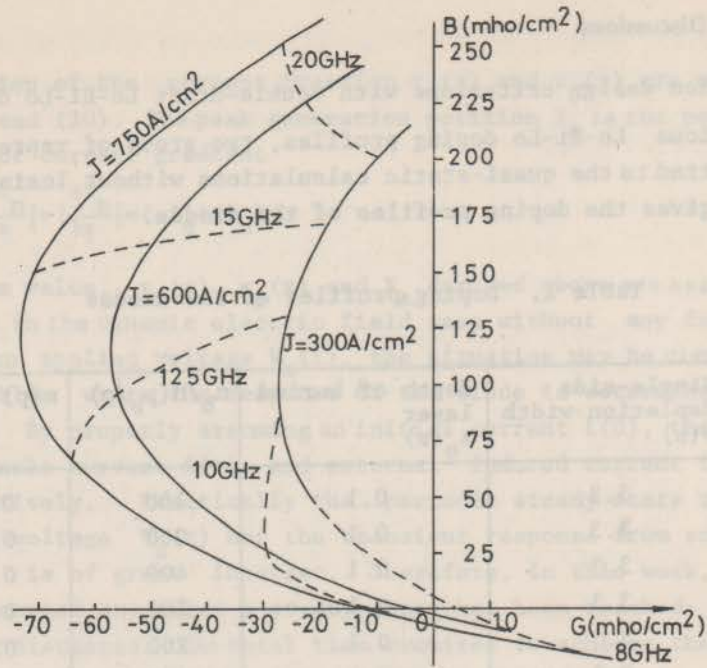


Fig. 2. Admittance diagram for diode 1-C at different dc bias current with modulation index  $m=20$ . (current tuning effect).

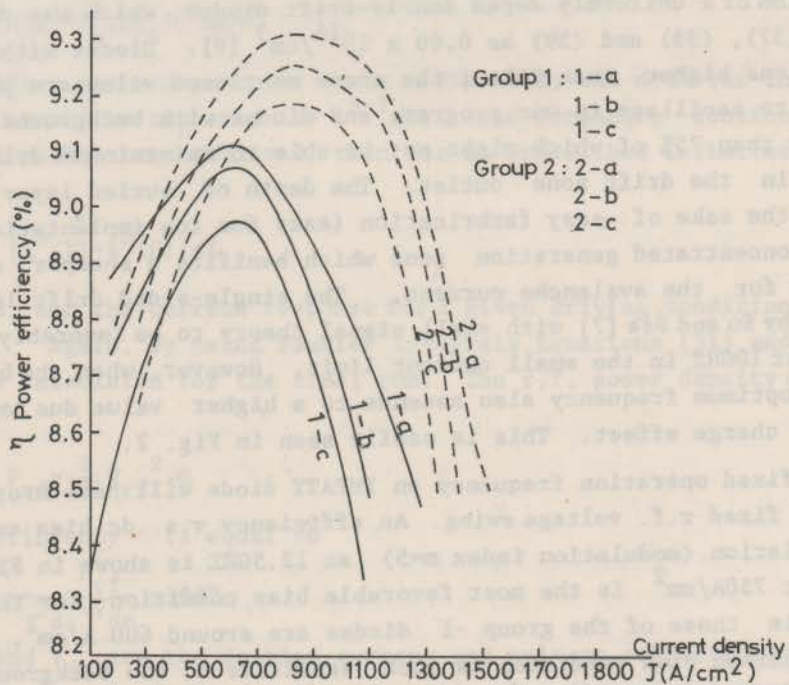


Fig. 3. Power efficiency as a function of current density for group 1 and group 2 diodes. Modulation index  $m=5$ , frequency  $f=12.5$  GHz.

$$f_r = \frac{1}{2\pi} \sqrt{\frac{2\alpha' J_{dc} v_{sl}}{\epsilon_s}} \quad (46)$$

where  $\alpha' = \frac{d\alpha}{dE}$ ,  $v_{sl}$  is the scattering-limited velocity of carriers. Since below  $6 \times 10^5$  V/cm,  $\alpha'$  is a monotonically increasing function of electric field [11], diodes of group -1 with higher critical field  $E_c$  than those of group -2, typically 1-C and 2-C shown in Fig. 4 and Fig. 5 respectively, would be biased at a lower current densities when operated at a specified frequency. In Appendix 1, we show that if space charge induced displacement current in the avalanche zone is considered, a factor 3 instead of 2 is obtained by means of the quasi-static method which is consistent with a rigorous small signal derivation of Gummel and Blue's [12].

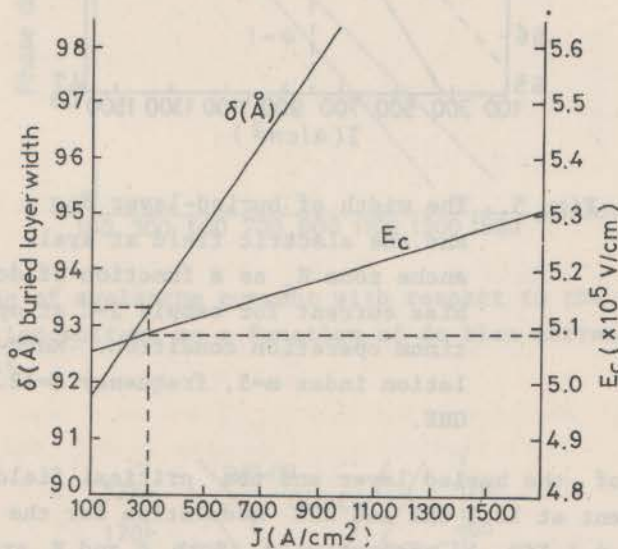


Fig. 4. The width of buried-layer  $\delta$ , and the electric field at avalanche zone  $E_c$  as a function of dc bias current for sample 1-C at optimum operation condition. Modulation index  $m=5$ , frequency  $f=12.5\text{GHZ}$ .

Comparison of two typical diodes 1-C and 2-C, which have different background concentrations but otherwise have the same doping profiles, would be interesting. For current densities greater than  $300 \text{ A/cm}^2$ , diode 2-C is the best choice of all at  $12.5\text{GHZ}$ . However, the power generation efficiency of 2-C drops very quickly at current densities less than  $300 \text{ A/cm}^2$ . Therefore diode 1-C becomes favorable at lower bias current condition.

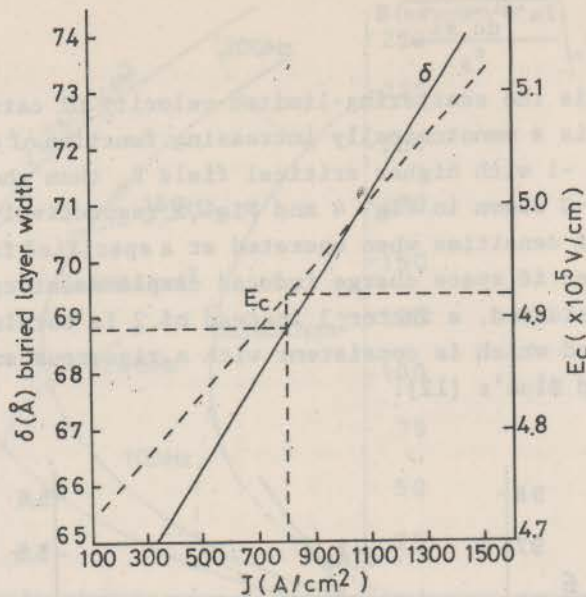


Fig. 5. The width of buried-layer  $\delta$ , and the electric field at avalanche zone  $E_c$  as a function of dc bias current for sample 2-C at optimum operation condition. Modulation index  $m=5$ , frequency  $f=12.5$  GHz.

The width  $\delta$  of the buried layer and the critical field  $E_c$  as a function of dc bias current at 12.5 GHz and 20% modulation for the diodes 1-C and 2-C are shown in Fig. 4 & Fig. 5, respectively. Both  $\delta$  and  $E_c$  are increasing functions of the bias current and have to be specified at its optimum condition. For instance, if diode 1-C is biased at  $300 \text{ A/cm}^2$ , the optimized buried layer width is about  $\delta=93.3 \text{ \AA}$  with a critical field  $E_c=5.09 \times 10^5 \text{ V/cm}$ ; and if diode 2-C is biased at  $750 \text{ A/cm}^2$ , the optimized  $\delta=68.8 \text{ \AA}$  and  $E_c=4.92 \times 10^5 \text{ V/cm}$ . Any deviation from these values would degrade the Lo-Hi-Lo-diodes efficiency significantly.

The avalanche current  $i(t)$  lags the r.f. voltage swing  $V_a(t)$  by about  $90^\circ$  by sharp pulse approximation derived by Read [13]. Actually, it is not so simple a case. The non-sinusoidal  $E_c(t)$  due to space charge effect of  $i(t)$  introduces deviation from ideal situation. The phase lags of diodes 1-a and 2-c is depicted in Fig. 6. As the bias current increases, the particle current starts earlier which would produce premature fall-off of the electric field and degrades the diode's efficiency. However, since the negative value of conductance increases linearly with current density as shown in Fig. 7, the maximum efficiency would occur at an intermediate value of bias current

density, which is shown in Fig. 3. The susceptance decreases with increasing current density. It is because the increase of the bias current introduces more inductive property and the diode becomes less capacitive.

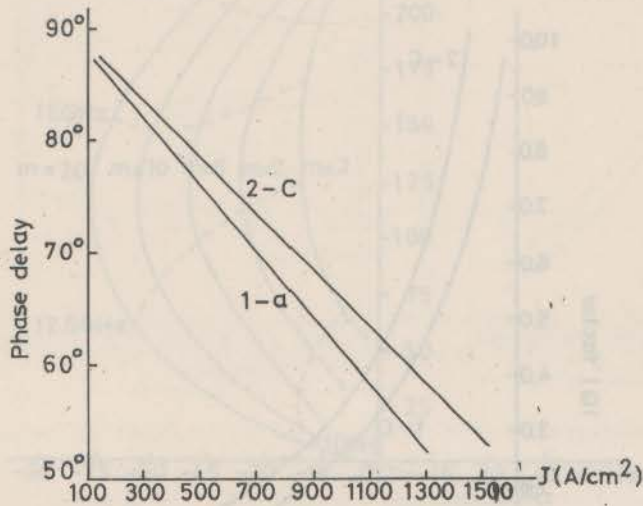


Fig. 6. Phase lag of avalanche current with respect to the applied oscillation voltage as a function of dc bias current, modulation index  $m=5$ .

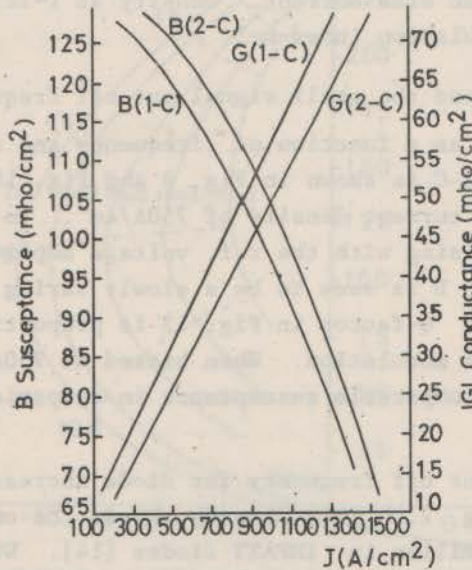


Fig. 7. Susceptance and Conductance as a function of dc bias current for sample 1-C and 2-C at  $f=12.5$  GHZ, modulation index  $m=5$ .

The negative value of the quality factor  $Q$  as a function of current density at  $f=12.5\text{GHZ}$  and 20% modulation is shown in Fig. 8. Referring to Fig. 7, it can be easily realized that the value  $Q=B/G$  should decrease with the increasing of current densities.

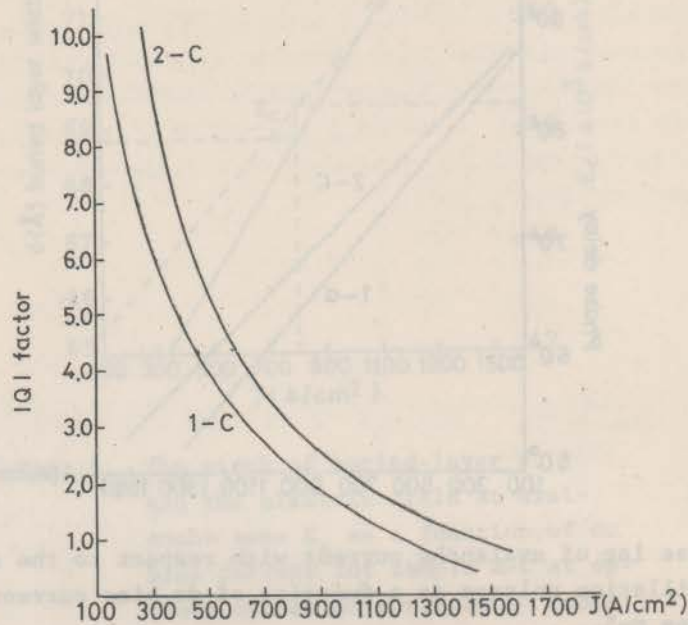


Fig. 8. Negative value quality factor as a function of dc bias current density at  $f=12.5\text{GH}$  with modulation index  $m=5$ .

## 2. Admittance diagram and the small signal cut off frequency

Diode's admittance as a function of frequency and r.f. voltage amplitude for the diodes 1-C and 2-C is shown in Fig. 9 and Fig. 10 respectively. Both diodes are biased at the current density of  $750\text{A/cm}^2$ . In general, conductance  $G$  is monotonically decreasing with the r.f. voltage amplitude as shown in Fig. 11, whereas susceptance  $B$  is seen to be a slowly varying function being shown in Fig. 12. The diode's  $Q$ -factor in Fig. 13 is proportional to the r.f. voltage amplitude up to 50% modulation. When biased at  $750\text{A/cm}^2$ , diode 2-C shows a lower conductance and comparable susceptance in comparison with those of the diodes 1-C.

The small signal cut off frequency for diode increases with bias current density is shown in Fig. 2. This clearly shows the current tuning effect, which has been very familiar in IMPATT diodes [14]. When the diodes 1-C is biased at  $600\text{A/cm}^2$ , the cut off frequency is about  $8.5\text{GHZ}$ . While bias current increases to  $750\text{A/cm}^2$ , the cut off frequency increases to  $9.5\text{GHZ}$ . At  $600\text{A/cm}^2$  bias, the maximum efficiency is obtained at  $12.5\text{GHZ}$ . With the bias

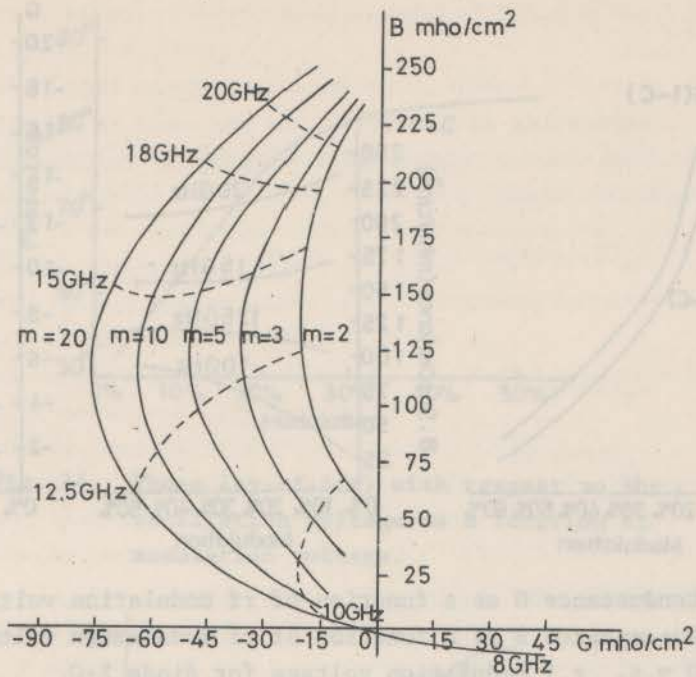


Fig. 9. Double-drift Lo-Hi-Lo silicon diode admittance as a function of frequency and voltage amplitude ( $m$  is defined as modulation index) with  $n=0.5146 \times 10^{16}/\text{cm}^3$ ,  $n_b=400n$ ,  $x_o=0.1\mu$ ,  $V_B=91.6\text{V}$ ,  $\delta=97\text{\AA}$ ,  $E_c=5.17 \times 10^5 \text{V/cm}$ , and current density  $J=750\text{A/cm}^2$ .

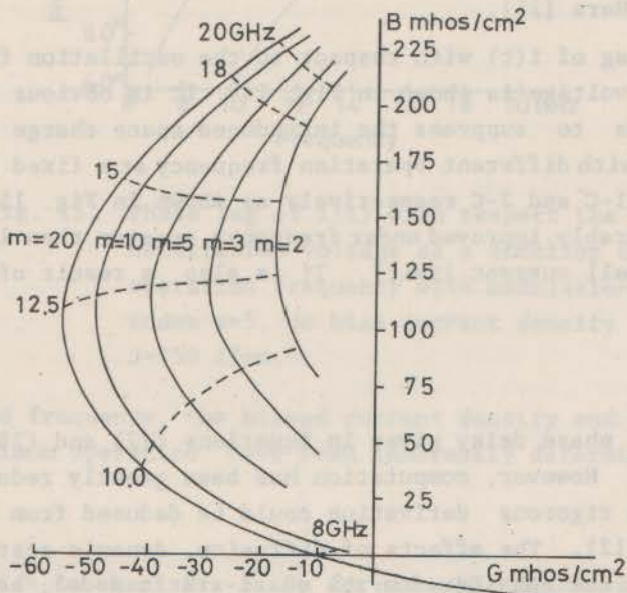


Fig. 10. Double-drift Lo-Hi-Lo silicon diode admittance as a function of frequency and ac voltage amplitude ( $m$  is defined as modulation index) with  $n=0.5832 \times 10^{16}/\text{cm}^3$ ,  $n_b=400n$ ,  $x_o=0.1\mu$ ,  $V_B=101.8\text{V}$ ,  $\delta=68\text{\AA}$ ,  $E_c=4.91 \times 10^5 \text{V/cm}$  and current density  $J=650\text{A/cm}^2$ .

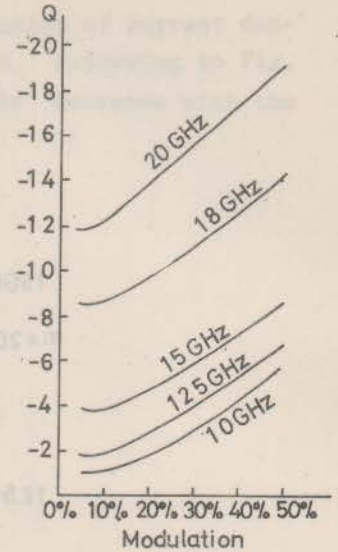
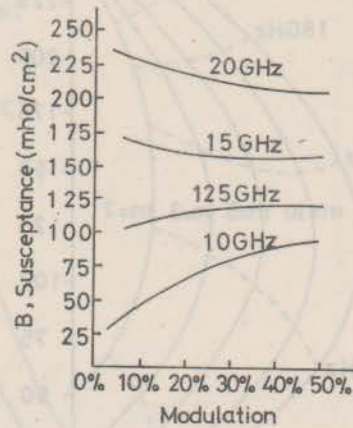
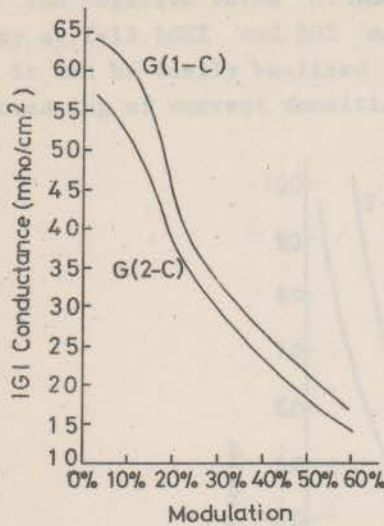


Fig. 11. Conductance  $G$  as a function of rf modulation voltage.

Fig. 12. Susceptance  $B$  as a function of rf modulation voltage for diode 2-C.

Fig. 13.  $Q$  v.s. r.f modulation voltage for diode 2-C.

increased to  $750\text{A}/\text{cm}^2$ , the optimum frequency moves to the region around 14 GHz. However, as shown in Fig. 9, increase of r.f. voltage leads to a slight decrease of optimum frequency, which is consistent with those reported by Grierson and O'Hara [15].

The phase lag of  $i(t)$  with respect to the oscillation field as a function of modulation voltage is shown in Fig. 14. It is obvious that a larger voltage swing tends to suppress the introduced space charge effect. Phase lag are also given with different operation frequency at a fixed bias current  $750\text{A}/\text{cm}^2$  for diodes 1-C and 2-C respectively as shown in Fig. 15. Phase relationship is considerably improved under frequency greater than 10 GHz (the optimum case in the small current limit). It is also a result of the current tuning effect.

## V. Conclusion

The linear phase delay given in Equations (27) and (28) is only approximately correct. However, computation has been greatly reduced with this simplification. A rigorous derivation could be deduced from a linearized small signal theory [12]. The effects of diffusion, dynamic scattering and dynamics early effect are not considered in the quasi-static model; however, these would be important for the designing of higher frequency (m-m wave) devices.

The current tuning effect, which cause on increase of optimum frequency with current density is crucial for designing a Lo-Hi-Lo diode. If diodes are



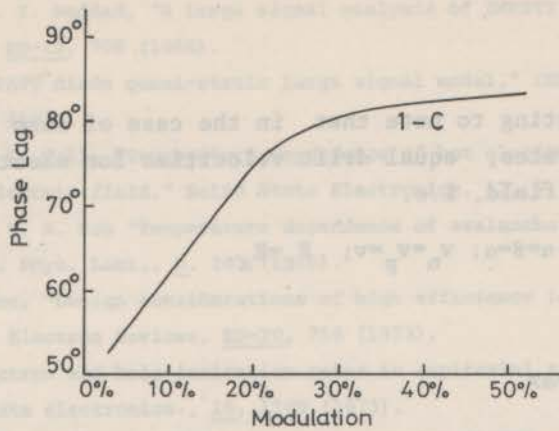


Fig. 14. Phase lag of  $i(t)$  with respect to the oscillation voltage as a function of modulation voltage.

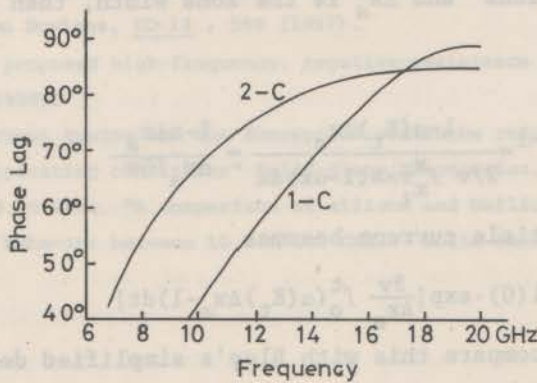


Fig. 15. Phase lag of  $i(t)$  with respect the oscillation voltage as a function of operation frequency with modulation index  $m=5$ , dc bias current density  $J=750$  A/cm.

operated at a fixed frequency, the biased current density and the buried layer width for the optimum operation have been inherently determined.

**Acknowledgment**

The authors wish to thank Dr. S. Su for valuable discussions, Mr. L.Chang for his cooperation in Program implementation and Mrs. M. C. Chang for her help in arranging the manuscript. Thanks are also due to the staffs of the computer Center of N. C. T. U. for their constant assistance throughout this

work.

### Appendix

It is interesting to note that in the case of zero saturation current, equal ionization rates, equal drift velocities for electrons and holes and a uniform avalanche field, i.e.

$$i_s \approx 0; \alpha = \beta = \alpha; v_n = v_p = v; E_t = E_a, \quad (\text{A-1})$$

we found

$$r_p(x) = \alpha x \quad (\text{A-2})$$

$$r_n(x) = 1 - \alpha x \quad (\text{A-3})$$

$$x_r - x_\ell = \Delta x_a \quad (\text{A-4})$$

in the avalanche zone and  $\Delta x_a$  is the zone width, then from Equation (18), we have

$$k = 2/3$$

$$(M\tau_i)^{-1} = \frac{1 - \alpha(E_t)\Delta x_a}{2/v \int_{x_\ell}^{x_r} \alpha x (1 - \alpha x) dx} = \frac{1 - \alpha \Delta x_a}{\Delta x_a / 3v} \quad (\text{A-5})$$

and the total particle current becomes

$$i(t) = i(0) \cdot \exp\left[\frac{3v}{\Delta x_a} \int_0^t (\alpha(E_t)\Delta x_a - 1) dt\right] \quad (\text{A-6})$$

However, when we compare this with Blue's simplified derivation [2].

$$i(t) = i(0) \cdot \exp\left[\frac{2v}{\Delta x_a} \int_0^t (\alpha(E_t)\Delta x_a - 1) dt\right] \quad (\text{A-7})$$

a factor of 3 instead of 2 is obtained by means of quasi-static method, so does the resonance frequency be corrected. The intrinsic response time has been corrected by the carrier induced displacement current in the avalanche zone. Blue had not taken this avalanche space-charge into account, that the particle current derived from his method might secure a slower growth rate than that of the real case.

### References

1. R. Kuvás and C. A. Lee, "Quasi-static approximation for semiconductor avalanches," *J. Appl. Phys.*, **41**, 1743 (1970).
2. J. L. Blue, "Approximate large signal analysis of IMPATT oscillators," *Bell Syst. Tech. J.*, **48**, 383 (1969).

3. W. J. Evans and G. I. Haddad, "A large signal analysis of IMPATT diodes," IEEE Trans. Electron Devices, ED-15, 708 (1968).
4. D. R. Decker, "IMPATT diode quasi-static large signal model," IEEE Trans. Electron Devices, ED-21, 469 (1974).
5. C. Y. Duh and J. L. Moll, "Temperature dependence of hot electron drift velocity in silicon at high electric field," Solid State Electronics, 11, 917 (1968).
6. C. R. Crowell and S. M. Sze "Temperature dependence of avalanche multiplication in semiconductors," Appl. Phys. Lett., 9, 242 (1966).
7. S. Su and S. M. Sze, "Design considerations of high efficiency low noise Si IMPATT diodes," IEEE Trans. Electron Devices, ED-20, 755 (1973).
8. W. N. Grant, "Electron and hole ionization rates in epitaxial silicon at high electric fields," Solid state electronics., 16, 1189 (1973).
9. L. Chang, Master Thesis, National Chiao-Tung University (1976).
10. M. Gilden and M. E. Hines, "Electronic tuning effects in the read microwave avalanche diode," IEEE Trans. Electron Devices, ED-13, 169 (1966).
11. S. Su, Ph.D. Thesis, National Chiao-Tung University (1975).
12. H. K. Gummel and J. L. Blue, "A small signal theory of avalanche noise in IMPATT diodes," IEEE Trans. Electron Devices, ED-14, 569 (1967).
13. W. T. Read, Jr., "A proposed high-frequency, negative-resistance diode", Bell System Tech. J., 37, 401 (1958).
14. J. R. Grierson, "Current tuning and the concept of avalanche resonance in IMPATT diodes under large signal operating conditions" Solid-State Electronics, 18, 459 (1975).
15. J. R. Grierson and S. O'Hara, "A comparison of silicon and Gallium Arsenide large signal IMPATT diode behavior between 10 and 100 GHz." Solid-State Electron. 16, 719 (1973).

Kalman [2] had shown that the optimization based on a quadratic performance functional for all initial states of an  $n$ -th order, linear regulator system requires that all  $n$  states be available for measurement. However, it is often not possible to measure every state variable in most of the chemical plants, and hence, the performance of any system with inaccessible states, in general, will be sub-optimal. The investigations of the problems concerned with the optimization of linear regulator systems with some inaccessible state variables are available elsewhere [3-13].

The optimal control theory gives a control law which is fully proportional feedback of the state, i.e. no integral action is obtained by the theory. This lack of integral action leads to an offset if an external disturbance occurs or if there is some modelling error. To eliminate this offset from a persistent change in the load, Koppal [14] suggested that an amount of integral action be parallel with the optimal control should be added in the design of a digital process controller.